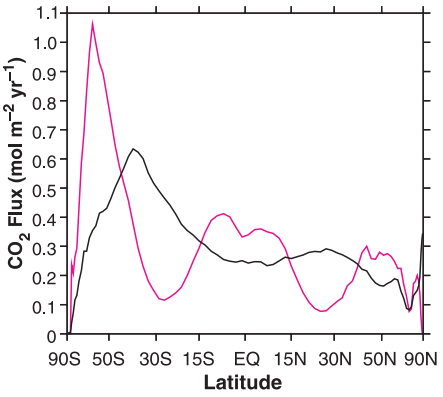

Fig. 3. Zonal mean anthropogenic CO_2 accumulation rate in the ocean (black line) and zonal mean anthropogenic CO_2 flux into the ocean (magenta line), by latitude band (averaged over land and ocean areas for 1995). The latitude axis is scaled so that equal horizontal distances represent equal areas on Earth's surface. On this scale, the total flux or accumulation into the ocean is proportional to the area under the appropriate curve. The Southern Ocean is an area with the highest anthropogenic CO_2 fluxes, but the Antarctic Convergence is the area with the largest anthropogenic CO_2 accumulation.

ern Ocean was much more vigorous in the period from ~1350 to 1880 A.D. than in the recent past. Our simulations reflect primarily late–20th century oceanographic conditions and support the conclusion of a subordinate role for deep convection in the Southern Ocean during this time period (*21*).

Our conclusion that present-day Southern Ocean uptake of anthropogenic carbon is large, but Southern Ocean storage is relatively small, has implications for the mechanisms governing future changes in the ocean carbon cycle. If most of the anthropogenic carbon entering the Southern Ocean is being transported northward isopycnally to the Antarctic Convergence, then a reduction in deep convection would have little impact on Southern Ocean uptake of anthropogenic carbon. Thus, the particular scenario described in (*6*) seems unlikely to occur. Changes in ocean circulation, reduction in sea ice coverage, temperature-dependent changes in CO_2 solubility, and changes in biological activity will impact oceanic CO_2 uptake (*6, 15*). Nevertheless, if global climate change reduces the density of surface waters in the Southern Ocean (*6, 15*), isopycnal surfaces that are now ventilated would become isolated from the atmosphere; this would tend to diminish Southern Ocean carbon uptake.

References and Notes

1. J. L. Sarmiento and E. T. Sundquist, *Nature* **356**, 589 (1992); C. D. Keeling, S. C. Piper, M. Heimann, in *Aspects of Climate Variability in the Pacific and Western Americas*, vol. 55 of *Geophysical Monograph Series*, D. H. Peterson, Ed. (American Geophysical Union, Washington, DC, 1989), pp. 305–363; P. P. Tans, I. Y. Fung, T. Takahashi, *Science* **247**, 1431 (1990).
2. C. L. Sabine *et al.*, *Global Biogeochem. Cycles* **13**, 179 (1999).
3. E. Maier-Reimer and K. Hasselmann, *Clim. Dyn.* **2**, 63 (1987).
4. U. Siegenthaler and J. L. Sarmiento, *Nature* **365,** 119 (1993).
5. J. L. Sarmiento, J. C. Orr, U. Siegenthaler, *J. Geophys. Res.* **97**, 3621 (1992); J. L. Sarmiento, C. Le Quere, S. W. Pacala, *Global Biogeochem. Cycles* **9**, 121 (1995).
6. J. L. Sarmiento, T. M. C. Hughes, R. J. Stouffer, S. Manabe, *Nature* **393**, 245 (1998).
7. N. Gruber, J. L. Sarmiento, T. S. Stocker, *Global Biogeochem. Cycles* **10,** 809 (1996).
8. N. Gruber, *Global Biogeochem. Cycles* **12**, 165 (1998).
9. A. Poisson and C.-T. Chen, *Deep Sea Res. Part A* **34**, 1255 (1987); P. P. Murphy, R. A. Freely, R. H. Gammon, K. C. Kelly, L. S. Waterman, *Mar. Chem.* **35**, 77 (1991).
10. P. B. Duffy and K. Caldeira, *Geophys. Res. Lett.* **24**, 1323 (1997); K. Caldeira and P. B. Duffy, *Geophys. Res. Lett.* **25**, 1003 (1998). Our simulations tend to have slow and shallow North Atlantic Deep Water, but they represent the Southern Ocean relatively well.
11. R. Pacanowski, K. Dixon, A. Rosati, *The G.F.D.L. Modular Ocean Model Users Guide version 1.0, GFDL Ocean Group Technical Report 2* (NOAA/Geophysical Fluid Dynamics Laboratory, Princeton, NJ, 1991).
12. J. M. Oberhuber, *J. Phys. Oceanogr.* **23**, 808 (1993).
13. P. B. Duffy, M. Eby, A. J. Weaver, *Geophys. Res. Lett.* **26**, 1739 (1999).
14. D. G. Martinson, *J. Geophys. Res.* **95**, 11641 (1990). The horizontal sizes of regions of brine-induced convection are very small in comparison to the grid cells in our model. Thus, a first-order representation of this subgrid-scale convection process is to sink rejected salt without mixing other tracers (*10, 13*).
15. F. Joos, G.-K. Plattner, T. F. Stocker, O. Marchal, A. Schmittner, *Science* **284**, 464 (1999); R. J. Matear and A. C. Hirst, *Tellus Ser. B* **51**, 722 (1999).
16. R. Wanninkhof, *J. Geophys. Res.* **97**, 7373 (1992).
17. S. Levitus and T. P. Boyer, *Temperature*, vol. 4 of *World Ocean Atlas 1994*, *NOAA Atlas NESDIS 4* (National Oceanographic Data Center, Silver Spring, MD, 1994).
18. K. Bryan, *J. Phys. Oceanogr.* **14**, 666 (1984).
19. Evidence of deep penetration of CFCs in the Southern Ocean [A. H. Orsi, G. C. Johnson, J. L. Bullister, *Prog. Oceanogr.* **43**, 55 (1999)] may appear to contradict the conclusions drawn here. However, CFCs equilibrate with the atmosphere much more rapidly than CO_2 does, and the solubility of CFCs is much more sensitive to changes in temperature than the solubility of CO_2 is. These two factors increase the ratio of CFC to anthropogenic CO_2 concentrations in the Southern Ocean.
20. W. S. Broecker, S. Sutherland, T.-H Peng, *Science* **286**, 1132 (1999).
21. These conclusions are echoed by a study showing deep convection to play a subordinate role in tracer transport in the North Atlantic [A. J. Watson *et al.*, *Nature* **401**, 902 (1999)].

22. We thank N. Gruber, R. M. Key, and C. L. Sabine for their insightful papers and access to the data underlying them. K.C. was supported by the NASA Oceanography Program and the U.S. Department of Energy Center for Research on Ocean Carbon Sequestration. P.B.D. was supported by the Lawrence Livermore National Laboratory Laboratory Directed Research and Development program.

15 July 1999; accepted 2 December 1999

Nanotube Molecular Wires as Chemical Sensors

Jing Kong,[1]* Nathan R. Franklin,[1]* Chongwu Zhou,[1] Michael G. Chapline,[1] Shu Peng,[2] Kyeongjae Cho,[2] Hongjie Dai[1]†

Chemical sensors based on individual single-walled carbon nanotubes (SWNTs) are demonstrated. Upon exposure to gaseous molecules such as NO_2 or NH_3, the electrical resistance of a semiconducting SWNT is found to dramatically increase or decrease. This serves as the basis for nanotube molecular sensors. The nanotube sensors exhibit a fast response and a substantially higher sensitivity than that of existing solid-state sensors at room temperature. Sensor reversibility is achieved by slow recovery under ambient conditions or by heating to high temperatures. The interactions between molecular species and SWNTs and the mechanisms of molecular sensing with nanotube molecular wires are investigated.

Carbon nanotubes are molecular-scale wires with high mechanical stiffness and strength. A SWNT can be metallic, semiconducting, or semimetallic, depending on its chirality (*1*). Utilization of these properties has led to applications of individual nanotubes or ensembles of nanotubes as scanning probes (*2, 3*), electron field emission sources (*4*), actuators (*5*), and nanoelectronic devices (*6*). Here, we report the realization of individual semiconducting-SWNT (S-SWNT)–based chemical sensors capable of detecting small concentrations of toxic gas molecules.

Sensing gas molecules is critical to environmental monitoring, control of chemical processes, space missions, and agricultural and medical applications (*7*). The detection of NO_2, for instance, is important to monitoring environmental pollution resulting from combustion or automotive emissions (*8*). Detection of NH_3 is needed in industrial, medical, and living environments (*9*). Existing electrical sensor materials include semicon-

[1]Department of Chemistry, [2]Department of Mechanical Engineering, Stanford University, Stanford, CA 94305, USA.

*These authors contributed equally to this work.
†To whom correspondence should be addressed. E-mail: hdai@chem.stanford.edu

ducting metal oxides (*7–9*), silicon devices (*10, 11*), organic materials (*12, 13*), and carbon black–polymer composites (*14*). Semiconducting metal oxides have been widely used for NO_2 and NH_3 detection (*7–9*). These sensors operate at high temperatures (200° to 600°C) in order to achieve enhanced chemical reactivity between molecules and the sensor materials for substantial sensitivity (*7*). Conducting polymers (*12*) and organic phthalocyanine semiconductors (*12, 13*) have also been investigated for NO_2 or NH_3 sensing. The former exhibit limited sensitivity (*12*), whereas the latter tend to have very high resistivity (sample resistance of >10 gigohms) (*13*). In this report, we show that the electrical resistance of individual semiconducting SWNTs change by up to three orders of magnitude within several seconds of exposure to NO_2 or NH_3 molecules at room temperature. Miniaturized chemical sensors based on individual SWNTs are thus demonstrated. Furthermore, we combine theoretical calculations with experiments to address the underlying fundamental question regarding how molecular species interact with nanotubes and affect their electrical properties.

Semiconducting SWNTs are chiral (m, n) tubes with $m - n \neq 3 \times$ integer. The band gap E_g of an S-SWNT scales with its diameter d as $E_g \sim 1/d$ ($E_g \propto 0.5$ eV for $d \sim 1.4$ nm) (*1*). It was previously found that when two metal contacts were used to connect an S-SWNT, the metal/S-SWNT/metal system exhibits *p*-type transistor characteristics with several orders of magnitude change in conductance under various gate voltages (*6, 15, 16*). Our nanotube chemical sensors were based on these S-SWNT transistors, obtained by controlled chemical vapor deposition growth of individual SWNTs from patterned catalyst islands on SiO_2/Si substrates (Fig. 1A) (*16, 17*). Gas-sensing experiments were carried out by placing an S-SWNT sample in a sealed 500-ml glass flask with electrical feedthrough and flowing diluted NO_2 [2 to 200 parts per million (ppm)] or NH_3 (0.1 to 1%) in Ar or air (flow rate of 700 ml/min) through the flask while monitoring the resistance of the SWNT.

We observed that the conductance of S-SWNT samples can be substantially increased or decreased by exposure to NO_2 or NH_3. A current versus voltage (I-V) curve recorded with an S-SWNT sample after a 10-min exposure to NH_3 showed an ~100-fold conductance depletion (Fig. 1B). Exposure to NO_2 molecules increased the conductance of the SWNT sample by about three orders of magnitude (Fig. 1C) when the SWNT sample was initially depleted by a back-gate voltage (V_g) of +4 V (*6, 15, 16*). The SWNT is a hole-doped semiconductor, as can be gleaned from the current versus gate voltage (I-V_g) curve shown in Fig. 2 (middle curve), where the conductance of the SWNT is observed to decrease by three orders of magnitude under positive gate voltages (*6, 15, 16*). The I-V_g curve recorded after the S-SWNT sample was exposed to NH_3 exhibits a shift of −4 V (Fig. 2, left curve). In contrast, the I-V_g curve was shifted by +4 V after NO_2 exposure (Fig. 2, right curve). The low resistance (~360 kilohms) of the SWNT under zero gate voltage suggests substantial hole carriers existing in the *p*-type nanotube at room temperature. Exposure to NH_3 effectively shifts the valence band of the nanotube away from the Fermi level, resulting in hole depletion and reduced conductance. For the NO_2 case, exposure of the initially depleted sample to NO_2 resulted in the nanotube Fermi level shifting closer to the valence band. This caused enriched hole carriers in the nanotube and enhanced sample conductance. These results show that molecular gating effects are capable of shifting the Fermi level of S-SWNTs and modulating the resistance of the sample by orders of magnitude.

The conductance of the SWNT sample increased sharply by about three orders of magnitude after 200 ppm of NO_2 was introduced (Fig. 3A). We investigated five S-SWNT samples and found that the response times (defined as time duration for resistance change by one order of magnitude) of the samples to 200 ppm of NO_2 were in the range of 2 to 10 s. The sensitivity [defined as the ratio between resistance after (R_{after}) and before (R_{before}) gas exposure] is ~100 to 1000. After the NO_2 flow was replaced by pure Ar, the conductance of the SWNT samples was observed to slowly recover, and the typical recovery time was ~12 hours. This suggests slow molecular desorption from the nanotube sample and that the SWNT chemical sensors can be reversibly used. Heating the exposed sample in air at 200°C led to recovery in ~1 hour. For comparison, a high-performance metal oxide sensor (Cd-doped SnO_2) operates at 250°C for detecting 100 ppm of NO_2 with a response time of ~50 s, a recovery time of ~8 min, and a sensitivity of ~300 (*8, 18*). A polypyrole-conducting polymer sensor can detect 0.1% NO_2 by an ~10% resistance change in ~5 to 10 min at room temperature (*12*). Thus, the S-SWNT sensors have the advantage of room temperature operation with sensitivity up to 10^3 over these materials.

NH_3-sensing results were obtained with the same SWNT sample after recovery from NO_2 detection (Fig. 3C). The conductance of the SWNT sample was observed to decrease ~100-fold after exposure to a 1% NH_3 flow. The response times to 1% NH_3 for five S-SWNT samples were ~1 to 2 min, and the sensitivity was ~10 to 100. For comparison,

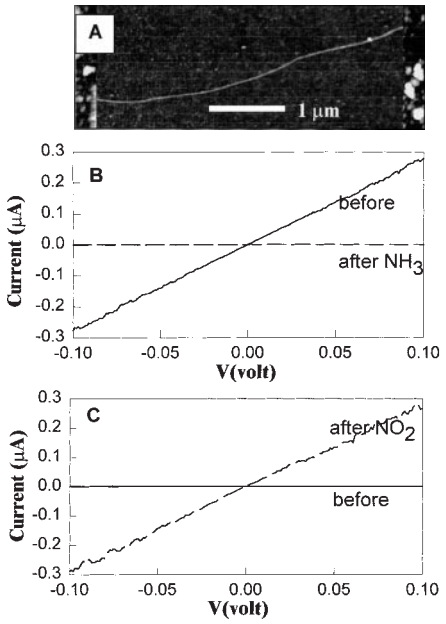

Fig. 1. Changes of electrical characteristics of a semiconducting SWNT in chemical environments. (**A**) Atomic force microscopy image of a metal/S-SWNT/metal sample used for the experiments. Nanotube diameter is ~1.8 nm. The metal electrodes consist of 20-nm-thick Ni, with 60-nm-thick Au on top. (**B**) Current versus voltage curves recorded before and after exposure to NH_3. (**C**) Current versus voltage curves recorded under $V_g = +4$ V, before and after NO_2 exposure.

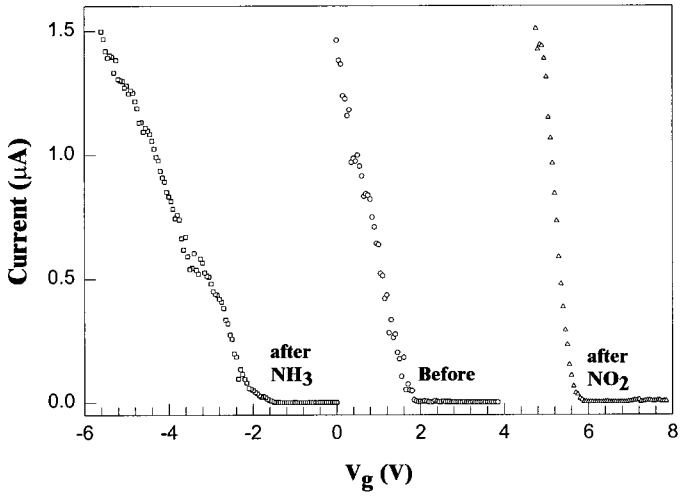

Fig. 2. Chemical gating effects to the semiconducting SWNT. Current versus gate voltage curves before NO_2 (circles), after NO_2 (triangles), and after NH_3 (squares) exposures. The measurements with NH_3 and NO_2 were carried out successively after sample recovery.

metal oxide NH_3 sensors typically operate at 300° to 500°C, with a response time of ~1 min and a sensitivity of ~1 to 100 toward 200 ppm to 1% NH_3 (*8*). Conducting polymer sensors can detect 1% NH_3 with a response time of ~5 to 10 min by an ~30% resistance change at room temperature (*12*).

For the S-SWNT samples, lowering the NO_2 concentration to 20 and 2 ppm led to response times of ~0.5 to 1 min and ~5 min, respectively (Fig. 3B). Lowering the concentration of NH_3 to 0.1% led to a response time of ~10 min (Fig. 3D). Thus, for detecting an ~10-fold resistance change of individual S-SWNT samples within minutes of gas exposure, the lower concentration limit is ~2 ppm for NO_2 and ~0.1% for NH_3. Similar sensing results were obtained when Ar or air was used as the carrier gas. This suggests that NH_3 or NO_2 dominates the response of the SWNT samples over molecules in the ambient environment. Over time, repeated sensing and recovery experiments with the S-SWNT samples obtained reproducible results.

To understand the chemical gating effects and the nanotube gas-sensing mechanism, we first considered the fact that S-SWNT samples appear to be hole doped (*p*-type) before the molecular sensing experiments. Hole doping in S-SWNTs has been observed by several groups (*6, 15, 16*). Possible hole-doping mechanisms include metal electrode–tube work function mismatch (*6*) and electrostatic effects due to charged species existing on the SiO_2 surface or bulk (*19*). Because our nanotubes are long (>3 μm), we suggested a hole-doping mechanism (for example, charged chemical groups on SiO_2) operating throughout the nanotube length. As a result of the hole doping, the Fermi level of an S-SWNT is typically located at ~25 meV above the valence band (*19*), which is responsible for the observed conductance of S-SWNT samples at room temperature (typical resistance of 300 kilohms to 5 megohms). Next, we considered the chemical nature of the molecules. NO_2 has an unpaired electron and is known as a strong oxidizer. Upon NO_2 adsorption, charge transfer is likely to occur from an SWNT to NO_2 because of the electron-withdrawing power of the NO_2 molecules. NH_3, on the other hand, is a Lewis base with a lone electron pair that can be donated to other species. However, it is necessary to investigate whether these qualitative pictures represent the correct mechanisms of molecular sensing with SWNTs.

We carried out first-principles calculations on molecule-SWNT complexes using density functional theory (*20*). NO_2 is found to bind with a semiconducting (10, 0) tube with an adsorption energy $E_a \sim 0.9$ eV (18.6 kcal/mol) and 0.1 electron charge transfer from the tube to a NO_2 molecule. Charge transfer from the nanotube to NO_2 should be the mechanism for increased hole carriers in an S-SWNT and enhanced conductance. For the NH_3-SWNT system, calculations found no binding affinity between NH_3 molecules and the (10, 0) tube. We suggest two possible indirect routes through which NH_3 molecules may affect S-SWNTs. The first is that NH_3 binds to hydroxyl groups on the SiO_2 substrate (*21*), which could partially neutralize the negatively charged groups on the SiO_2 surface and lead to positive electrostatic gating to the S-SWNT. Second, interactions may exist between NH_3 molecules and an SWNT through other species. It was previously found that NH_3 can interact strongly with adsorbed oxygen species on graphite (*22*). Preadsorbed oxygen species on a nanotube could interact with NH_3 and affect its electrical properties. These possible mechanisms require further experimental and theoretical investigations.

We also investigated the electrical properties of metallic SWNTs in various chemical environments. A metallic tube was identified by small changes in the conductance with gate voltage (a typical resistance of ~20 to 200 kilohms) (*16*). We found that, for a typical metallic SWNT, exposure to NO_2 or NH_3 increased or decreased, respectively, the conductance of the sample by ≤30%. The explanation for these small changes is that, for a metallic SWNT, small shifts of the Fermi level do not result in a substantial change in the density of states at the Fermi level and, thus, in the charge carriers in the nanotube.

The interactions between NO_2 and NH_3 with graphite have been previously investigated (*22–25*). For SWNTs, molecular interaction effects have been studied in the case of Br and I intercalation with bulk samples of SWNT ropes (*26, 27*). The intercalation leads to substantially enhanced sample conductance (*26*, *27*). Our report is concerned with molecular interactions with individual semiconducting and metallic

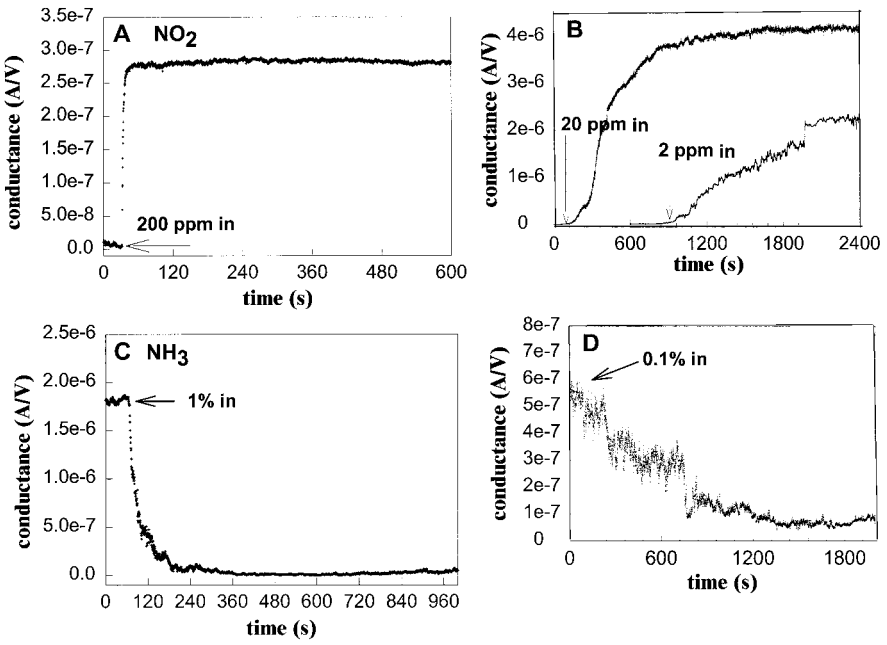

Fig. 3. Electrical response of a semiconducting SWNT to gas molecules. (**A**) Conductance (under $V_g = +4$ V, in an initial insulating state) versus time in a 200-ppm NO_2 flow. (**B**) Data for a different S-SWNT sample in 20- and 2-ppm NO_2 flows. The two curves are shifted along the time axis for clarity. (**C**) Conductance ($V_g = 0$, in an initial conducting state) versus time recorded with the same S-SWNT sample as in (A) in a flow of Ar containing 1% NH_3. (**D**) Data recorded with a different S-SWNT sample in a 0.1% NH_3 flow. Read 3.5e-7, for example, as 3.5×10^{-7}.

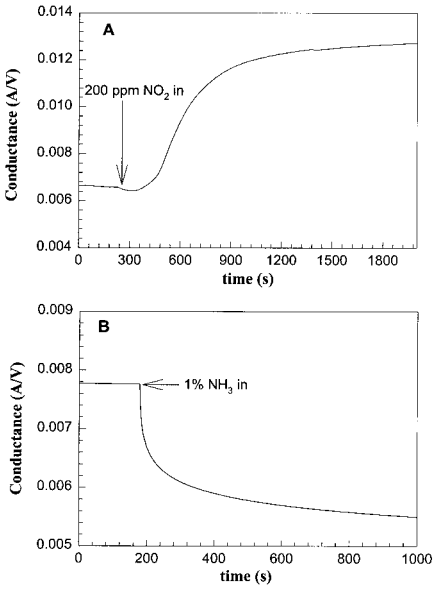

Fig. 4. Electrical response of bulk SWNT mats to NO_2 and NH_3 molecules. (**A**) Conductance versus time data recorded with an SWNT mat in 200 ppm of NO_2. (**B**) Conductance versus time recorded with an SWNT mat in 1% NH_3.

SWNTs. We have also investigated the effects of NO_2 and NH_3 on the electrical properties of mats of SWNT ropes made from as-grown laser ablation materials. In a 200-ppm NO_2 flow, the resistance of an SWNT mat is found to decrease from $R = 150$ to 80 ohms ($R_{before}/R_{after} \sim 2$) in ~10 min (Fig. 4A). In a 1% NH_3 flow, the resistance of a second SWNT mat increases from 120 to 170 ohms ($R_{after}/R_{before} \sim 1.5$) in ~10 min (Fig. 4B). In these bulk SWNT samples, the molecular interaction effects are averaged over metallic and semiconducting tubes. Also, the inner tubes in SWNT ropes are blocked from interacting with NO_2 and NH_3 because the molecules are not expected to intercalate into SWNT ropes. This explains the small resistance change of bulk SWNT mats by gas exposure compared to that of an individual S-SWNT.

The main feature of individual S-SWNT sensors, besides their small sizes, is that they operate at room temperature with sensitivity as high as 10^3. An individual nanotube sensor can be used to detect different types of molecules. The selectivity is achieved by adjusting the electrical gate to set the S-SWNT sample in an initial conducting or insulating state. The fast response of a nanotube sensor can be attributed to the full exposure of the nanotube surface area to chemical environments. Thus, nanotube molecular wires should be promising for advanced miniaturized chemical sensors.

References and Notes

1. M. S. Dresselhaus, G. Dresselhaus, P. C. Eklund, *Science of Fullerenes and Carbon Nanotubes* (Academic Press, San Diego, CA, 1996).
2. H. Dai, J. H. Hafner, A. G. Rinzler, D. T. Colbert, R. E. Smalley, *Nature* **384**, 147 (1996).
3. S. Wong, E. Joselevich, A. Woolley, C. Cheung, C. Lieber, *Nature* **394**, 52 (1998).
4. W. A. de Heer, A. Chatelain, D. Ugarte, *Science* **270**, 1179 (1995).
5. R. H. Baughman *et al.*, *Science* **284**, 1340 (1999).
6. S. Tans, A. Verschueren, C. Dekker, *Nature* **393**, 49 (1998).
7. Special issue on Gas-Sensing Materials, *MRS Bull.* **24** (1999).
8. Y. Shimizu and M. Egashira, *MRS Bull.* **24**, 18 (1999).
9. Y. Takao, K. Miyazaki, Y. Shimizu, M. Egashira, *J. Electrochem. Soc.* **141**, 1028 (1994).
10. H. M. McConnell *et al.*, *Science* **257**, 1906 (1992).
11. A. Mandelis and C. Christofides, *Physics, Chemistry and Technology of Solid State Gas Sensor Devices* (Wiley, New York, 1993).
12. J. Miasik, A. Hooper, B. Tofield, *J. Chem. Soc. Faraday Trans. 1* **82**, 1117 (1986).
13. S. Capone, S. Mongelli, R. Rella, P. Siciliano, L. Valli, *Langmuir* **15**, 1748 (1999).
14. M. C. Longergan *et al.*, *Chem. Mater.* **8**, 2298 (1996).
15. R. Martel, T. Schmidt, H. R. Shea, T. Hertel, P. Avouris, *Appl. Phys. Lett.* **73**, 2447 (1998).
16. T. Soh *et al.*, *Appl. Phys. Lett.* **75**, 627 (1999).
17. J. Kong, H. Soh, C. F. Quate, H. Dai, *Nature* **395**, 878 (1998).
18. G. Sberveglieri, S. Groppelli, P. Nelli, *Sens. Actuators* **B4**, 457 (1991).
19. C. Zhou, J. Kong, H. Dai, in preparation.
20. S. Peng and K. Cho, in preparation.
21. M. L. Hair, *Infrared Spectroscopy in Surface Chemistry* (Dekker, New York, 1967).
22. A. Cheng and W. A. Steele, *J. Chem. Phys.* **92**, 3867 (1990).
23. P. Sjovall, S. K. So, B. Kasemo, R. Franchy, W. Ho, *Chem. Phys. Lett.* **172**, 125 (1990).
24. P. Rowntree, G. Scoles, J. Xu, *J. Chem. Phys.* **92**, 3853 (1990).
25. P. A. Heiney, *J. Phys. Chem. Solids* **53**, 1333 (1992).
26. R. S. Lee, H. J. Kim, J. E. Fischer, A. Thess, R. E. Smalley, *Nature* **388**, 255 (1997).
27. L. Grigorian *et al.*, *Phys. Rev. Lett.* **80**, 5560 (1998).

28. We thank J. Han, L. Yang, and M. Tang for discussions. Supported by NSF, Defense Advanced Research Projects Agency/Office of Naval Research, Petroleum Research Fund of the American Chemical Society, Semiconductor Research Cooperation, the Camile and Henry Dreyfus Foundation, and the Laboratory for Advanced Materials at Stanford University.

1 October 1999; accepted 24 November 1999

Single-File Diffusion of Colloids in One-Dimensional Channels

Q.-H. Wei,*† C. Bechinger,* P. Leiderer

Single-file diffusion, prevalent in many processes, refers to the restricted motion of interacting particles in narrow micropores with the mutual passage excluded. A single-filing system was developed by confining colloidal spheres in one-dimensional circular channels of micrometer scale. Optical video microscopy study shows evidence that the particle self-diffusion is non-Fickian for long periods of time. In particular, the distribution of particle displacement is a Gaussian function.

Single-file diffusion (SFD) occurs when the individual pores of the medium are so narrow that the particles are unable to pass each other (*1, 2*). The sequence of particles remains unchanged over time, and thus, the basic principle of diffusion as a physical mixing process comes into question. The concept of SFD was originally introduced more than 40 years ago in biophysics to account for the transport of water and ions through molecular-sized channels in membranes (*3*); since then, in addition to biological systems (*4, 5*), SFD is also discussed in the context of interaction of Markov chains in statistics (*6*), the transportation of adsorbate molecules through zeolites (*2*), and charge-carrier migration in one-dimensional (1D) polymer and superionic conductors (*7*). Furthermore, SFD is also related to surface growth phenomena through some mapping (*8*).

As the mutual passage of particles is prohibited in single-filing (SF) systems, the movements of individual particles are correlated, even at long time periods, because the displacement of a given particle over a long distance necessitates the motion of many other particles in the same direction. This correlation is reflected in the long-time behavior of the mean-square displacement (MSD), which has been predicted for an infinite system to be (*6, 7, 9–11*)

$$\langle \Delta x^2 \rangle = 2F\sqrt{t} \qquad (1)$$

where F is the SF mobility and t is time. Accordingly, SFD processes, in contrast to 2D and 3D self-diffusion seen in colloidal systems (*12*), cannot be described by a diffusion coefficient; that is, the SFD does not obey Fick's laws.

Experimental evidence confirming non-Fickian behavior was unavailable for a long time because of the lack of ideal experimentally accessible SF systems. Recently, measurements of SFD became feasible in artificial crystalline zeolites. Adsorbate molecules, like methane or CF_4 with diameters of 3.8 and 4.7 Å, respectively, confined in $AlPO_4-5$ zeolite with a pore size of 7.3 Å, are considered to be good realizations of SF systems. Although some experimental evidence for the occurrence of SFD was found by pulsed field gradient nuclear magnetic resonance study (*13, 14*), some results from different groups and experimental methods are still in contradiction, even for the same system (*15, 16*), as indicated by Hahn and Kärger (*17*), who suggest and explore several possible reasons. Other effects, such as attractive particle interaction (*18*), the possible existence of correlations between particles of neighboring pores (*19*), have also been shown to play a vital role in the mechanism and rates of intracrystalline diffusion. Because of the shortage of structural information on the atomic level, the mechanism of molecular diffusion in zeolites, however, is still under debate.

We created a well-defined SFD model system by confining paramagnetic colloidal spheres of several micrometers in a set of circular trenches fabricated by photolithography. The channels are well-characterized, and the particle-particle interaction can be precisely adjusted by an external magnetic field. Moreover, because the time and length scales in such a colloidal system are easily accessed

Faculty of Physics, University of Konstanz, Postfach M676, D-78457 Konstanz, Germany.

*To whom correspondence should be addressed. E-mail: qwei+@pitt.edu (Q.-H.W.) and clemens.bechinger@uni-konstanz.de (C.B.)

†Present address: Department of Physics and Astronomy, University of Pittsburgh, Pittsburgh, PA 15260, USA.